Biochimica et Biophysica Acta 1798 (2010) 344–353

Contents lists available at ScienceDirect

Biochimica et Biophysica Acta

journal homepage: www.elsevier.com/locate/bbamem

Structural characterization of the transmembrane proximal region of the hepatitis C virus E1 glycoprotein

Roberta Spadaccini [a,b,*], Gerardino D'Errico [a,c], Viviana D'Alessio [a], Eugenio Notomista [d], Alessia Bianchi [e], Marcello Merola [d,e,*], Delia Picone [a,*]

[a] Dipartimento di Chimica, Università degli Studi di Napoli "Federico II", Via Cintia, 80126 Napoli, Italy
[b] Dipartimento di Scienze Biologiche ed Ambientali, Università del Sannio, Via Port'Arsa 11, 82100, Benevento, Italy
[c] CSGI, Consorzio interuniversitario per lo sviluppo dei Sistemi a Grande Interfase, Italy
[d] Dipartimento di Biologia Strutturale e Funzionale, Università degli Studi di Napoli "Federico II", Via Cintia, 80126 Napoli, Italy
[e] Novartis V&D, via Fiorentina 1, 53100 Siena, Italy

ARTICLE INFO

Article history:
Received 11 May 2009
Received in revised form 16 October 2009
Accepted 27 October 2009
Available online 3 November 2009

Keywords:
HCV
NMR
ESR
Pretransmembrane region
E1 glycoprotein

ABSTRACT

A detailed knowledge of the mechanism of virus entry represents one of the most promising approaches to develop new therapeutic strategies. However, viral fusion is a very complex process involving fusion glycoproteins present on the viral envelope. In the two hepatitis C virus envelope proteins, E1 and E2, several membranotropic regions with a potential role in the fusion process have been identified. Among these, we have selected the 314–342 E1 region. Circular Dichroism data indicate that the peptide exhibits a clear propensity to adopt a helical folding in different membrane mimicking media, such as mixtures of water with fluorinated alcohols and phospholipids, with a slight preference for negative charged bilayers. The 3D structure of $E1_{314–342}$ peptide, calculated by 2D-NMR in a low-polarity environment, consists of two helical stretches encompassing residues 319–323 and 329–338 respectively. The peptide, presenting a largely apolar character, interacts with liposomes, as indicated by fluorescence and electron spin resonance spectra. The strength of the interaction and the deepness of peptide insertion in the phospholipid membrane are modulated by the bilayer composition, the interaction with anionic phospholipids being among the strongest ever observed. The presence of cholesterol also affects the peptide–bilayer interaction, favoring the peptide positioning close to the bilayer surface. Overall, the experimental data support the idea that this region of E1 might be involved in membrane destabilization and viral fusion; therefore it may represent a good target to develop anti-viral molecules.

1. Introduction

Hepatitis C virus (HCV) is a major public health problem worldwide, as it is a major cause of chronic hepatitis, cirrhosis, and hepatocellular carcinoma [1]. Currently there is no vaccine to prevent HCV infection and the available therapeutic agents not only have limited success but produce several side effects [2]. A detailed understanding of the mechanism of HCV virus entry could provide a molecular basis for the development of new therapeutic strategies [3], however little is known about the events that mediate membrane fusion and cell entry for HCV. HCV is an enveloped virus that belongs to the hepacivirus genus of the *Flaviviridae* family [4]. The viral genome is an approximately 9.6 kb long single stranded positive RNA molecule that is translated into a polyprotein precursor of about 3010 amino acids. The precursor is co- and post-translationally processed by cellular and viral proteases to produce at least 10 proteins [5]. The first three N-terminal products, Core and the two envelope glycoproteins E1 and E2, represent the structural proteins, while the remaining part of the genome encodes for the non-structural proteins [5]. Among these NS3, NS4 (A and B) and NS5 (A and B) include all the essential replicative functions, such as the helicase and the polymerase, and the portion of the viral genome encoding this proteins can autonomously replicate, as demonstrated by the establishment of sub-genomic replicons [6]. The small proteins p7 and NS2 separate these two regions. Both proteins have been found essential for the generation of infectious particles, although their role and localization remain elusive [7,8].

The two envelope proteins E1 (residues 192 to 383) and E2 (residues 384 to 746 for genotype 1) are essential for receptors binding

Abbreviations: CD, circular dichroism; CHOL, cholesterol; COSY, correlated spectroscopy; DLPC, dilauroyl phosphatidylcholine; DLPG, dilauroyl phosphatidylglycerol; DOPC, dioleoyl phosphatidylcholine; DOPG, dioleoyl phosphatidylglycerol; ESR, electron spin resonance; HCV, hepatitis C virus; HFIP, hexafluoroisopropanol; MLV, multilamellar vesicles; NMR, nuclear magnetic resonance; NOESY, nuclear Overhauser effect spectroscopy; *n*-PCSL, spin-labeled phosphatidylcholine; SDS, sodium dodecyl sulfate; SUV, small unilammelar vesicle; TFE, trifluoroethanol; TM, transmembrane region of the viral glycoprotein; TOCSY, total correlation spectroscopy

* Corresponding authors. R. Spadaccini is to be contacted at Fax: +39081674409. D. Picone, Fax: +39081674409. M. Merola, Fax: +390577 243512.
E-mail addresses: rspadacc@unisannio.it (R. Spadaccini), marcello.merola@novartis.com (M. Merola), picone@unina.it (D. Picone).

0005-2736/$ – see front matter © 2009 Elsevier B.V. All rights reserved.
doi:10.1016/j.bbamem.2009.10.018

and fusion with the host cell membrane [9,10]. E1 and E2 are glycosylated in their large N-terminal ectodomains, while are anchored to the virus membrane by their C-terminal hydrophobic regions. Through their transmembrane (TM) domains E1 and E2 form a heterodimer stabilized by noncovalent interactions [11]. This oligomer is thought to be the prebudding form of the functional complex [12], which is present at the surface of HCV particles [13] and is involved in viral entry. Progress in the understanding of viral entry have been achieved after the establishment of: (a) a retrovirus expression system generating pseudoparticles carrying HCV glycoproteins (HCVpp) [14] and (b) full-length genome based on genotype 2a producing infectious particles in cell culture (HCVcc) [15–17]. The host membrane spanning protein CD81, previously identified as putative HCV receptor [18], has been found to be essential but not sufficient for infection. The involvement of other identified candidate receptors to the mechanism of productive infection, such as SR-BI, class B, type I scavenger receptor, LDL-R, low density lipoprotein receptor, and the last identified Claudin 1 and Occludin [19,20], has been shown in different situations, but the precise topology of the event is still lacking. Interestingly, while E2 is the viral protein responsible for CD81 binding, HCVpp carrying E2 but deprived of E1 are unable to infect cells [9,21]. Thus, E1E2 heterodimer formation, or an even higher organized structure containing both the proteins, is a prerequisite for the formation of a functional complex. Viral entry has been found to be a pH dependent process and it has been supposed that, analogously to the fusion mechanism of more or less related viruses, low endosomal pH promotes the rearrangement of E1/E2 to an active form [22].

Based on the classification of HCV in the Flaviviridae family, its envelope glycoproteins could be included in the class II fusion proteins [23], however the identification of either E1 or E2 as the HCV fusion protein is still very controversial. Nevertheless, studying the interaction of peptide libraries of HCV envelope proteins with model membranes, several regions in E1 and E2 with potential fusion activity have been identified, suggesting that distinct segments in the two glycoproteins can be involved in the fusion process. In particular, on the E1 glycoprotein, at least three regions, encompassing the residues 265–296, 310–340 and 349–381 respectively, have been shown to interact with model membranes [24–26].

These data support the idea that the mechanism of virus fusion is very complex. Indeed it is already known that, apart from the fusion peptide, there exist other membranotropic segments along the sequence of membrane fusion proteins which, under a concerted action, are essential for membrane fusion [27]. In particular several studies with viral fusion proteins have shown that the pretransmembrane regions play a pivotal role in membrane fusion and viral entry [28].

Interestingly, the regions proximal to the TM domains, that are usually rich in aromatic amino acids, demonstrate strong tendencies to partition into membrane interfaces contributing to the destabilization of the membranes necessary for fusion [29,30]. This has been widely reported in the literature for class I fusion proteins [31–34]. Another important feature of pretransmembrane regions is that peptides derived from such domains can also be used to develop fusion inhibitors, as already shown for the pretransmembrane domain of gp41 [30].

Although class II fusion proteins present evident differences with respect to class I ones, it is likely that pretransmembrane domains act in a similar way, being actively involved in the fusion process [24].

In this work we report the identification and structural investigation of a putative pretransmembrane region of the E1 envelope glycoprotein of HCV. The NMR solution structure of the peptide has been solved in media mimicking the low-polarity conditions of the membrane environment and its interaction with membrane model systems has been studied through CD, fluorescence and ESR spectroscopies.

The experimental results support the hypothesis that the selected region of E1 may have a role in the complicated sequence of events leading to membrane fusion and virus entry.

2. Material and methods

2.1. Materials

The $E1_{314–342}$ was purchased from the Universitè de Lausanne (Institut de Biochimie, Ch. Des Boveresses 155, CH-1066-Epalinges). After purification by HPLC, the sample purity was checked by mass spectrometry and found >95%. SDS, TFE, dichloromethane and methanol, HPLC-grade solvents, as well as hexafluoroisopropanol (HFIP) and d_2-HFIP were purchased from Sigma.

The phospholipids dioleoyl phosphatidylcholine (DOPC), dioleoyl phosphatidylglycerol (DOPG), dilauroyl phosphatidylcholine (DLPC) and dilauroyl phosphatidylglycerol (DLPG), were purchased from Avanti Polar Lipids. Spin-labeled phosphatidylcholine (*n*-PCSL) with the nitroxide group at different positions, *n*, in the *sn*-2 acyl chain were also purchased from Avanti Polar Lipids. The spin-labels were stored at −20 °C in ethanol solutions at a concentration of 1 mg/ml. Cholesterol (CHOL) was obtained from Sigma.

2.2. Structure prediction

The secondary structure of E1 was predicted using Jpred3, a multiple alignment-based consensus method (http://www.compbio.dundee.ac.uk/~www-jpred/), HNN (http://npsa-pbil.ibcp.fr/cgi-bin/npsa_automat.pl?page=npsa_nn.html), NNPredict (http://www.cmpharm.ucsf.edu/~nomi/nnpredict.html), SSPro (http://www.igb.uci.edu/?page=tools&subPage=psss), SAM-T02 (http://compbio.soe.ucsc.edu/HMM-apps/T02-query.html) and JUFO (http://www.meilerlab.org/web/), which are neural networks-based methods, PHYRE (http://www.sbg.bio.ic.ac.uk/~phyre/) and PredictProtein (http://www.predictprotein.org/) which are collections of secondary structure analysis algorithms including PHDhtm [35], which provides a prediction of transmembrane helices topology.

2.2.1. Circular dichroism

All CD spectra were recorded using a JASCO J-715 spectropolarimeter with a cell of 1.0 mm path length. CD measurements were performed at 298 K, using a wavelength range from 260 to 190 nm, 1 nm bandwidth, 10 accumulations, and 10 nm/min of scanning speed. The concentration of the peptide in all the solutions was 0.1 mM. Spectra were processed with JASCO software, baseline corrected, and smoothed using a third-order least-square polynomial fit. The secondary structure content was estimated with various deconvolution methods by using DICHROWEB tools (http://www.cryst.bbk.ac.uk/cdweb/) [36].

2.3. NMR spectrometry

The samples for NMR spectroscopy were prepared by dissolving the appropriate amount of peptide in 0.5 ml of solution to obtain a peptide concentration of 1.0 mM. The composition of the water/d_2-HFIP mixture for NMR measurements was 20/80 by volume.

NMR spectra were recorded on a Bruker DRX-600 spectrometer equipped with a cryoprobe. One-dimensional (1D) NMR spectra were recorded in the Fourier mode with quadrature detection, and the water signal was suppressed by low-power selective irradiation in the homogated mode. DQF-COSY, TOCSY, and NOESY experiments [37–40] were run in the phase-sensitive mode using quadrature detection in ω_1 by time-proportional phase increase of the initial pulse. Data block sizes were 2048 addresses in t_2 and 512 equidistant t_1 values. Before Fourier transformation, the time domain data matrices were multiplied by shifted $\sin^2$ functions in both dimensions. A mixing time of

70 ms was used for the TOCSY experiments. NOESY experiments were run at 300 K with mixing times in the range of 100–250 ms. The qualitative and quantitative analysis of NMR spectra was achieved using the NMRVIEW software [41].

2.4. Structure calculation

Peak volumes were translated into upper distance bounds with the routine CALIBA of the CYANA software [42].

The necessary pseudoatom corrections were applied for nonstereospecifically assigned protons at prochiral centers and for the methyl group of aliphatic side chains. After the redundant and duplicated constraints were discarded, the final list for the structure of $E1_{314–342}$ in HFIP/water included 386 constraints, which were used to generate an ensemble of 100 structures by the standard protocol of simulated annealing in torsion angle space implemented in CYANA (using 10,000 steps). No dihedral angle restraints and no hydrogen bond restraints were applied. The best 40 structures, the one with the lowest values of the target functions, were refined by *in vacuo* minimization in the AMBER 1991 force field, using the program SANDER of the AMBER 6.0 suite [43]. To mimic the effect of solvent screening, all net charges were reduced to 20% of their real value, and a distance-dependent dielectric constant ($\varepsilon = r$) was used. The cutoff for nonbonded interactions was 12 Å. The NMR-derived upper bounds were imposed as semiparabolic penalty functions, with force constants of 16 kcal mol^{-1} $Å^{-2}$; the function was shifted to linearity when the violation exceeded 0.5 Å.

2.5. Liposome sample preparation

Liposomes incorporating $E1_{314–342}$ in the lipid bilayer were prepared as follows. The peptide was dissolved in HFIP. The lipids were dissolved in a dichloromethane/methanol mixture (2:1 v/v). Appropriate amounts of these mother solutions were thoroughly mixed in round-bottom sample tubes by vortexing. For ESR measurements small aliquots of the spin-labeled lipid solution in ethanol were also added to the mixture. A thin film of the peptide–lipid mixture was produced by evaporating the solvent with dry nitrogen gas. Final traces of solvent were removed by subjecting the sample to vacuum desiccation overnight. The samples were then hydrated with the due amount of 50 mM phosphate water solution, pH 4.5 and vortexed, obtaining a suspension of multi-lamellar vesicles (MLV), which were directly used for ESR measurements. To perform CD and fluorescence measurements, small unilamellar vesicles (SUV), preferred for their lower scattering, were obtained from multilamellar ones by sonication for 10 min with a Microson XL instrument equipped with a microtip, alternating 30 s sonication and 30 s ice-cooling to avoid overheating of the sample. By this procedure $E1_{314–342}$ was incorporated in liposomes formed by DOPC, DOPG, DLPC, DLPG, DOPC/CHOL (1:5 molar ratio) and DOPG/CHOL (1:5 molar ratio).

2.6. Fluorescence measurements

Incorporation of the peptide in lipid bilayers was investigated by monitoring the changes in the Trp fluorescence emission spectra. SUV samples to be analyzed contained 5×10^{-6} M $E1_{314–342}$, and the lipid at peptide/lipid molar ratio 1:100. Fluorescence measurements were performed at 25 °C using a Fluorolog-3 spectrofluorimeter (Jobin Yvon). The excitation wavelength was 280 nm and emission spectra were recorded between 300 and 420 nm, at slit widths of 2 nm.

2.7. ESR measurements

For ESR experiments, MLV dispersions, in the absence and in the presence of $E1_{314–342}$, were obtained as described above, and transferred into a 100 μl glass capillary, which was immediately flame-sealed. Sample to be analyzed contained 3×10^{-3} M phospholipid and $E1_{314–342}$ at a peptide/phospholipid mole ratio ranging between 0.004 and 0.2. In all samples, the spin-label content was 1/100 by mole of the lipid concentration.

ESR spectra were recorded on a 9 GHz Bruker Elexys E-500 spectrometer. The capillaries were placed in a standard 4 mm quartz sample tube. All the measurements were performed at 25 °C. Spectra were recorded using the following instrumental settings: sweep width, 120 G; resolution, 1024 points; time constant, 20.48 ms; modulation frequency, 100 KHz; modulation amplitude, 1.0 G; incident power, 6.37 mW. Several scans, typically 32, were accumulated to improve the signal-to-noise ratio. Values of the outer hyperfine splitting, $2A_{max}$, were determined by measuring the difference between the low-field maximum and the high-field minimum, through a homemade, MATLAB-based software routine. In general, $2A_{max}$ is dependent on both the amplitude (i.e., order) and rate of lipid chain rotational motion [44], and is therefore a useful parameter for characterizing chain dynamics in phospholipid membranes. The main source of error on the $2A_{max}$ value is the uncertainty in composition of samples prepared by mixing few microliters of mother solutions. For this reason, reproducibility of $2A_{max}$ determination was estimated by evaluating its value for selected independently prepared samples with the same nominal composition. It was found to be ± 0.2–0.3 G.

2.8. Accession codes

The chemical shifts and the coordinates of the $E1_{314–342}$ peptide have been deposited in BMRB and PDB databases with accession codes 16477 and 2knu respectively.

3. Results

The region of E1 to analyze was defined by prediction of the secondary structure of E1 using several methods, including multiple alignment-based consensus methods, neural networks, and algorithms, which provide a prediction of transmembrane helices topology.

All the methods predicted the existence of a region located at the C-terminal, about 70 residues long, with a helical content ranging from 50% to 95%, depending on the algorithm used. Within this region, PHDhtm [35] identified two transmembrane helices, 18 and 25 residues long respectively, separated by a 5 residues loop. Drawing a consensus from all the predictions, reported in Fig. 1A, the existence of three helical regions—H1, H2 and H3—could be hypothesized in the C-terminal domain of E1. H1 is the shortest and the most hydrophilic helix, whereas H2 and H3 are more hydrophobic and show the features of transmembrane helices. The helical wheel representations of the three helices (Fig. 1B) show that all of them are amphipathic—although the amphipathic region of H3 is very short, with H1 and H2 showing the highest hydrophobic moments.

Two short sequences in the middle of both H2 and H3—the sequences RIP and VGN, respectively—showed lower helix propensity than the surrounding regions and could represent bends or less regular regions within the two long helices.

On the basis of the predictions we first tried to express in *E. coli* several constructs encompassing H1, H2 and H3 helices, but unfortunately we could not obtain a suitable amount of protein, probably owing to the intrinsic toxicity of these fragments leading eventually to cellular death (data not shown) [45], therefore we decided to switch to shorter synthetic peptides. Planning to study the (pre)transmembrane region of E1, the most logic choice would have been to synthesize a peptide spanning the whole helices H1 and H2 but, because of the technical difficulties in getting the very hydrophobic peptide enough pure for spectroscopic analysis, we decided to investigate first the structural features and the membrane

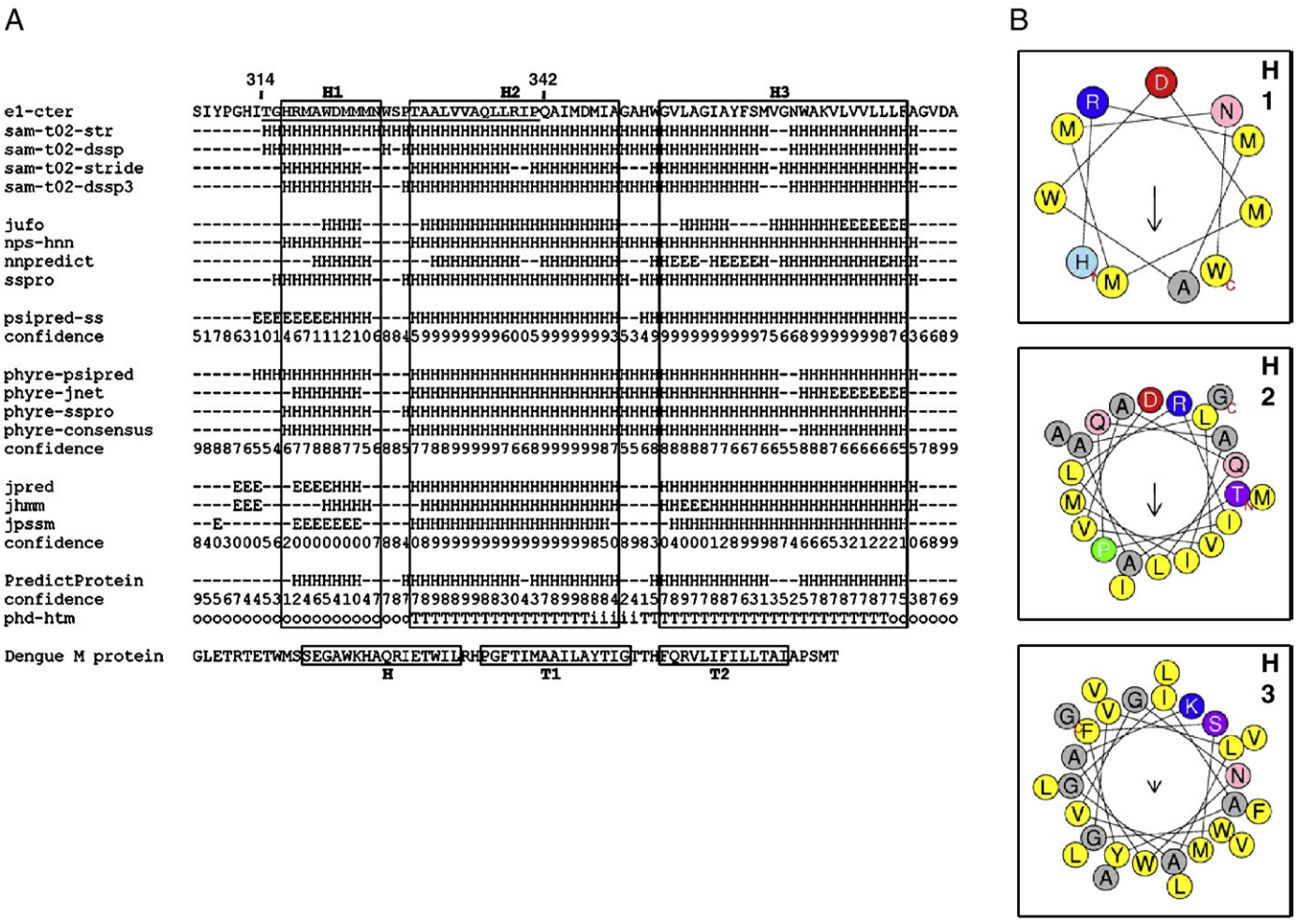

Fig. 1. (A) Sequence and secondary structure prediction of the C-terminal region of the E1 protein. The peptide analyzed in this study is shown in bold. Sequence and secondary structure for the C-terminal region of the M protein of the Dengue virus are shown for comparison. (B) Helical wheel representation of H1 (hydrophobicity = 0.68; hydrophobic moment = 0.42), H2 (hydrophobicity = 0.71; hydrophobic moment = 0.38), and H3 (hydrophobicity = 0.94; hydrophobic moment = 0.14).

interaction of a shorter synthetic peptide corresponding to the 314–342 region of E1, spanning the entire H1 helix and the first half of helix H2, up to the low helix propensity-middle region of H2. It is interesting to notice that this sequence is highly conserved in all HCV genotypes as reported in the sequence alignment in Table 1.

To characterize the secondary structure of $E1_{314–342}$, we examined the far UV-CD spectra in several solvent systems mimicking different biological environments, represented by saline buffers, SDS micelles and water/fluorinated alcohols mixtures. In aqueous solution the peptide is completely soluble only at acidic pH. The spectrum of the peptide in acetate buffer, pH 4.5 (Fig. 2A), shows a broad minimum around 216 nm, suggesting the presence of an extended conformation. We have also explored the peptide conformation in low polarity mixtures represented by water and fluorinated alcohols—such as TFE (data not shown) and HFIP—with different composition, and found in general a prevailing helical conformation, with the two characteristic minima around 208 and 222 nm, the helical percentage—calculated as reported in the methods section—ranging from 20% in the 30/70 water/HFIP mixture up to 25% in the 80/20 mixture. Fig. 2A reports the CD spectra acquired in water/HFIP 70/30, 50/50 and 20/80 by volume. A similar percentage of helical content (23%) was found also in presence of SDS at pH 4.5 (Fig. 2A), whereas the helix amount decreases at higher pH values. The CD spectra in SDS at different pH values together with the spectrum in TFE/water 50/50 are reported as Supplementary material (Figure S1). In order to simulate the bilayer composition, we considered also a variety of phospholipids (zwitterionic vs. anionic ones, saturated vs. unsaturated ones), eventually in combination with cholesterol, as it has been shown that cholesterol play a major role in the fusion process operated by many enveloped viruses [46] and specifically by HCV [22]. Concerning the CD curves of $E1_{314–342}$ in liposomes, reported in Fig. 2B, the spectrum obtained in DOPC at pH 4.5 presents a broad minimum around 220 nm, indicating the presence of an extended conformation. Whereas in the negatively charged DOPG multilamellar vesicles show the typical minima associated with helical structures, and a helix content as high as 65% is observed. The CD spectra are not influenced by the presence of

Table 1
Sequence alignment of residues 314–342 from reference strains of the six major HCV genotypes and the E1 preTM sequence used in this work.

Genotype	Strain	
1a	H77C	TGHRMAWDMMMNWSPTAALVVAQLLRIPQ
1b	NC1	TGHRMAWDMMMNWSPTAALVVSQLLRIPQ
5a	SA13	TGHRMAWDMMMNWSPTTALVMAQLLRIPQ
3a	NZL1	–GHRMAWDMMMNWSPAVGMVVAHVLRLPQ
2c	BEBE1	TGHRMAWDMMMNWSPTTTMLLAYLVRIPE
4a	ED43	TGHRMAWDMMMNWSPTTTLVLAQVMRIP–
6a	HK	TGHRMAWDMMMNWSPTATLVLSSILRVPE
E1preTM		^{314}TGHRMAWDMMMNWSPTAAL**V**VAQ**L**LRIPQ^{342}
Consensus		**********:. :::: ::*:*

The residues highlighted in bold are the one whose mutation blocks or reduces viral entry [65]. The sequence alignment was done with the program CLUSTALW.

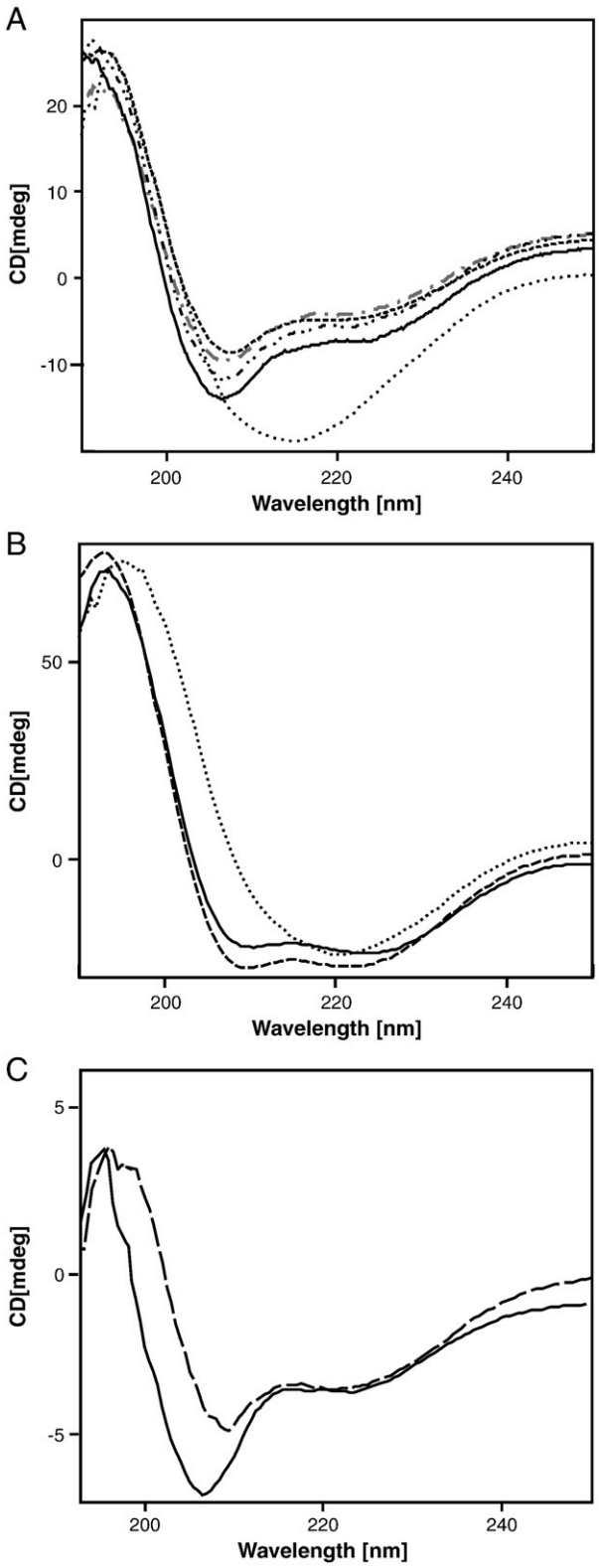

Fig. 2. (A) CD spectra of $E1_{314-342}$ in sodium acetate buffer, pH 4.5 (dotted line), HFIP/water (80:20 v/v) (continuous line), HFIP/water (70:30 v/v) (dashed double dotted line), HFIP/water (50:50 v/v) (gray dashed-dotted line), SDS 100 mM in phosphate solution (dashed line), (B) spectra in DOPG vesicles (dashed line), DLPG vesicles (continuous line), DOPC (dotted line), (C) DOPC/CHOL (dashed line), DOPG/CHOL (continuous line).

unsaturations along the phospholipid acyl chains, as the spectrum in DLPG is very similar to that in DOPG, with a helical content of around 60% (Fig. 2B).

Strikingly, the spectra obtained when cholesterol is added to either the DOPG and DOPC bilayer (Fig. 2C) are very similar, and suggest that cholesterol induces a conformational change in the peptide, independently on the lipid charge. It is worth to observe that all the measurements were carried-out at acidic pH in order to be closer to fusogenic conditions [22].

Overall, the data reported in Fig. 2 indicate that the conformation of the peptide is strongly dependent on the chemical–physical features of the environment, as in the case of several other viral TM domains [47], and that the SDS/negative liposomes interaction and helical folding requires neutralization of acidic residues, like in the case of the C-terminal acidic alpha helix of NS4A from HCV [48].

NMR spectra were initially acquired in SDS micelles, pH = 4.5, trying to reproduce a negatively charged micellar environment similar to that of DOPG vesicles. Unfortunately the quality of NMR spectra in SDS was very poor, with very broad lines. The same behavior was observed in the mixture TFE/H_2O, probably because the higher sample concentrations required for NMR experiments favors the presence of peptide aggregates, thus preventing a detailed conformational analysis in these conditions. For this reason, on the basis of the CD data, we selected the HFIP water 80/20 mixture to study the three-dimensional structure of the peptide in detail, by using a standard 2D NMR based approach. In these experimental conditions, based on the spectrum quality, and also in comparison with previous studies on linear peptides of similar size, we could confidently assume that the peptide was monomeric.

According to the preliminary CD study, the NOESY spectra show the typical connectivities of a mainly helical conformation. The overview of the sequential and medium-range NOE effects in HFIP/H_2O, reported in the bar diagram in Fig. 3A, shows the presence of several NOEs contacts diagnostic of a helical conformation from residue 328 to residue 339. In particular, a continuous pattern of dαN (1,1+3) and d (NN) contacts between residue 332 and 339 indicates the presence of a α helical structure, although the presence in the same region of dαN(i, i+2) contacts suggests the presence of mixed helical conformations. On the other hand several NOE effects diagnostic of helical structures are present also in the region encompassing residues 328–331, suggesting the hypothesis of a continue helix from Pro328 to Arg 339, but some breaks due to peaks overlap prevented the possibility to detect unambiguously the NOE involving residues 329–331.

Another small helical turn is present between residue Trp 320 and Met 323 and a few NOEs diagnostic for a helical conformation are present also between His 316 and Ala 319, but the severe signal overlapping at the N-terminus prevented the possibility to identify clearly a helical conformation. The region between Met 324 and Ser 327 does not show NOEs diagnostic of any ordered conformation; thus the whole structure can be described as a helix-break-helix motif.

To obtain information about the solvent exposure of the single residues, we performed a deuterium exchange experiment by dissolving the freeze-dried peptide directly into an 80/20 HFIP/D_2O mixture. The TOCSY spectrum acquired after 12 h indicated that the amide protons of residues from Ala 330 and Leu 338 were still detectable in solution, whereas all the remaining signals disappeared completely. This result, reported also in the bar-diagram, suggests that between the two helical stretches, the one at the N terminus is more flexible and in fast deuterium exchange regime, whereas the helix at the C terminus is more rigid.

To check for the presence of proline isomerization we analyzed connectivities between Ser 327 and Pro 328 and between Ile 340 and Pro 341. The dαα(i,i+1) cross-peaks, typical for the *cis* conformer, were missing, whereas we could observe dαδ(i,i+1) connectivities for both prolines, indicating that they are both in a *trans* conformation.

The whole set of 386 NOE derived distance constraints was used as input for structure calculation, as described in detail in the experimental section. From the 100 structures calculated the 40 with the

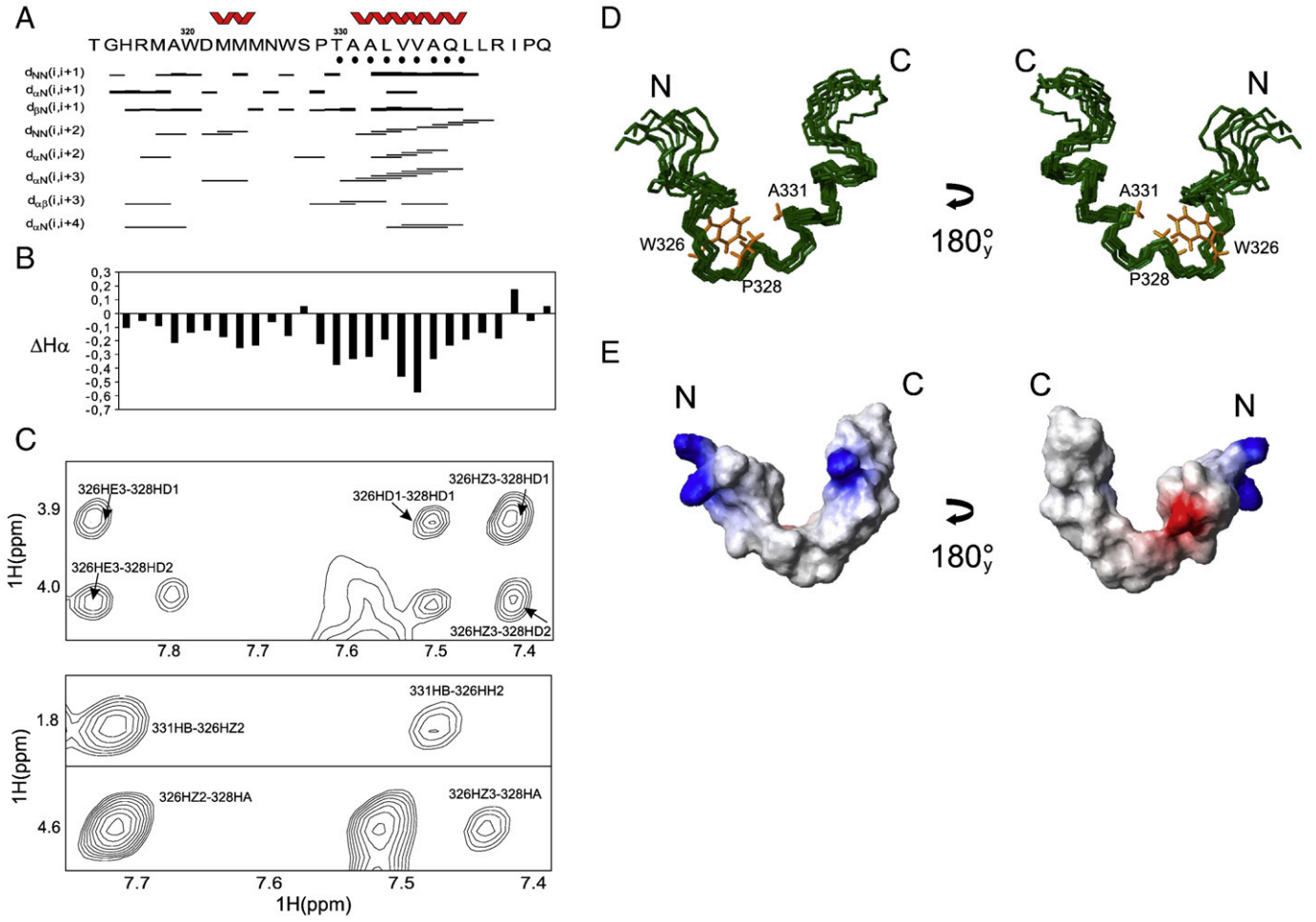

Fig. 3. (A) Bar diagram reporting the sequential and medium range NOE effects in the NOESY spectra recorded in the HFIP/H2O (80:20) mixture at 298 K, the filled circles indicate residues whose amide protons do not exchange with deuterium after 24h. (B) 1Hα chemical shift differences versus peptide sequence. The differences were calculated subtracting the experimental values to the random coli conformation values reported by [67]. (C) NOE contacts between the side chains of Trp 326 and PRO 328 and ALA 331 respectively in the 100 ms NOESY 2D spectrum. (D) Bundle of the best 10 structures calculated of the $E1_{314–342}$. In yellow are shown the side chains of Trp 326, Pro 328 and Ala 331. (E) Electrostatic surface representation of the lowest energy structure of the $E1_{314–342}$ peptide.

lowest target function were energy minimized with AMBER 6. The bundle of the 10 lowest energy structures resulting from this procedure, shown in Fig. 3D, was selected as representative of the solution structure of the $E1_{314–342}$ peptide, a structural statistics table of the calculated ensemble is presented as supplemental material. The best fit between the structures was found when the more flexible N and C terminal residues were excluded, i.e. between Met 318 and Leu 338. To give an idea of the structure quality, the calculated RMSD of the backbone atoms and of all heavy atoms for the 10 lowest energy structures, were 0.52 and 0.89 Å, respectively.

According to the qualitative analysis based on the bar-diagram, the refined structure can be described as two helical stretches, a short one spanning from Ala 319 to Met 323 and a second, longer helix from Thr 329 to Leu 338. Unfortunately the great number of overlapping signals in N-terminal part does not allow a better definition of this region, but the presence of a longer helical segment cannot be excluded as suggested from the difference between the measured Hα chemical shift and the random coils reported in Fig. 3B. The two helices are interrupted by a bend centered on Trp 326. This region is very well conserved in all the conformers and is mainly stabilized from side chain contacts like the one between the side chains of Trp 326 and Pro 328, and Trp 326 and Ala 331 (some of them are shown in Fig. 3C). Despite the fact that the HFIP/H_2O solution does not favor hydrophobic interaction, many NOE contacts between these side chains are observed, also at low mixing times, suggesting that these conformers are highly populated.

The analysis of the electrostatic potential surfaces (Fig. 3E) indicates that the helical region is mainly hydrophobic, with almost all the charged residues located near the N-terminus. This organization suggests that at least part of the peptide could easily interact with membrane double layer.

To evaluate the membrane interaction tendency of $E1_{314–342}$ we used tryptophan fluorescence spectroscopy. Indeed the fluorescence intensities of some fine vibronic structures in the tryptophan spectrum show strong environmental dependence [49,50]. In particular, the emission maximum shifts from 350 to 329 nm when going from water to an apolar medium such as dioxane [49]. The quantum yield might also undergo large changes whose direction and extent depend on the system under consideration [51]. Consistently, the fluorescence experiments allow evaluating if $E1_{314–342}$ is embedded in the DOPC, DOPG, DOPC/CHOL and/or DOPG bilayer by measuring a change in the polarity experienced by the tryptophans.

As shown in Fig. 4, $E1_{314–342}$ in buffer presents a Trp emission spectrum typical of the aqueous environment ($\lambda_{max} = 348$ nm), indicating that both Trp are exposed to the aqueous medium. In DOPC and, even more, in DOPG SUV dispersions, the emission maximum is shifted to lower wavelength ($\lambda_{max} = 340$ nm for DOPC and 333 nm for DOPG), indicating the peptide tryptophans to be embedded in a less

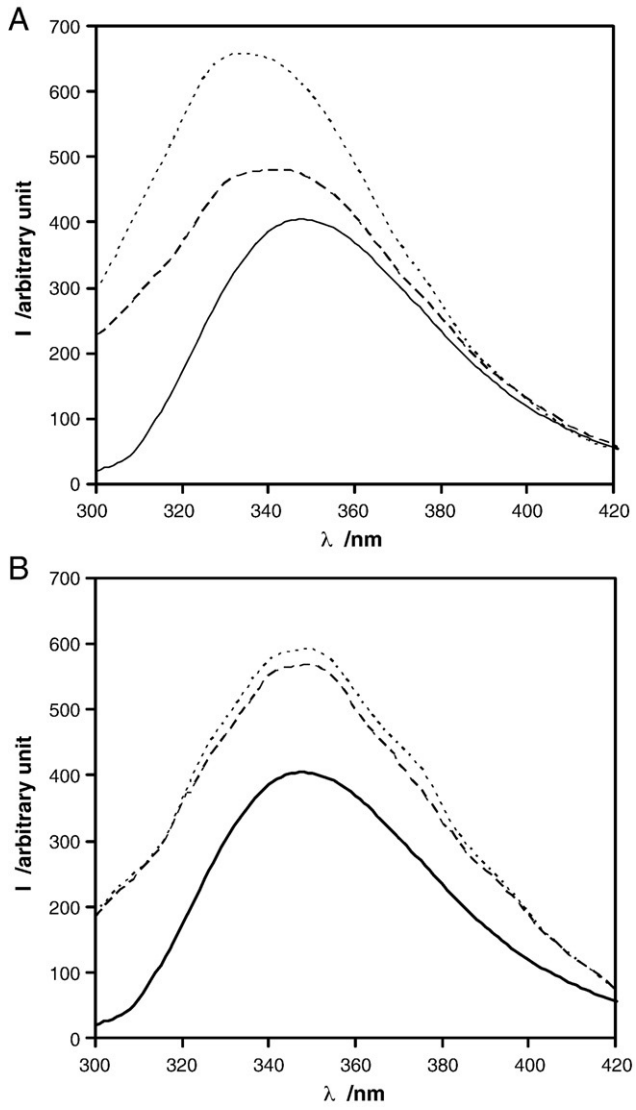

Fig. 4. (A) tryptophan emission spectra of $E1_{314–342}$ in aqueous medium at pH 4.5 (solid line), and in the presence of DOPC (dashed line), DOPG (dotted line) liposomes. (B) Tryptophan emission spectra of $E1_{314–342}$ in aqueous medium at pH 4.5 (solid line), and in the presence of DOPC/CHOL (dashed line), DOPG/CHOL (dotted line) liposomes.

polar environment. Particularly, in the case of DOPG, the experimental evidences indicate that the peptide is effectively incorporated in the lipid bilayer. In contrast, in DOPC/CHOL and DOPG/CHOL SUV dispersions the emission maximum remains at values very close to that observed in water ($\lambda_{max} = 348$ and 349 nm, respectively), an evidence that the peptide's tryptophans are exposed to the aqueous medium. In all cases, the quantum yield increases; this effect was already observed for other peptides, derived from fusion glycoproteins, interacting with model membranes [24,52–54].

Analogously to the CD spectra, the fluorescence spectra are not influenced by the presence of unsaturations along the phospholipid acyl chains, as the spectra in DOPC and DLPG are very similar to those observed in DOPC and DOPG, respectively (spectra not shown).

The association of the $E1_{314–342}$ with the membranes was further investigated by ESR spectroscopy. This technique requires the presence of unpaired electrons in the systems to be investigated. In ESR silent systems, spin-labeled substances can be purposely introduced. Cyclic nitroxides are very often used as spin-labeling moieties due to their remarkable stability. Analysis of their spectra allows to investigate the polarity of the microenvironment in which the label is embedded and restrictions in its motion determined by microviscosity and/or by specific interactions with the system components. This approach has proved to be fruitful to the study of the interactions between peripheral as well as integral proteins and membranes. Either the protein/peptide or the lipid can be labeled, so that the system can be studied by different "points of view" [55]. Particularly, ESR spectroscopy of spin-labeled lipids is a well assessed method, developed by Marsh et al. [56–58], allowing to evaluate the perturbation of the lipid chain mobility due to proteins/peptides interaction with the membrane. Good results are usually obtained by using bilayers in the fluid-phase state [59] because changes in the lipid mobility due to the interaction are enhanced.

In the present work we have investigated spin-labeled phosphatidylcholines (*n*-PCSL) incorporated in either DLPC or DLPG membranes, in the absence and in the presence of the peptide $E1_{314–342}$ (1:10 mol/mol peptide to lipid ratio). At room temperature, both DLPC and DLPG bilayers are in the fluid-phase state [60]. The *n*-PCSL spectra in the zwitterionic and the anionic lipid samples are shown in Fig. 5A and B, respectively. In general, a nitroxide ESR signal presents three hyperfine lines, due to the coupling between the electron spin and the nuclear spin of the nitrogen atom. Insertion of the label in a locally oriented ordered environment such as a membrane causes the appearance of a spectral anisotropy, detectable by the splitting of the lateral lines. Inspection of the figures shows that, for both lipids, in the absence of peptide, the spectrum anisotropy becomes progressively less evident with increasing *n*, as the spin-label position is stepped down the chain toward the center of the membrane. In fact, as opposed to the clearly defined axially anisotropic spectra that are obtained for 5-PCSL, where the label is positioned on the acyl chain close to the phospholipid polar headgroup, a sharp, three-line, quasi-isotropic spectrum is obtained for 12-PCSL, bearing the label close to the terminal methyl region of the chain. This flexibility gradient is a characteristic hallmark of the liquid-crystalline state of fluid phospholipid bilayers [58]. In Fig. 5A slight, but significant perturbations in DLPC bilayers due to the presence of $E1_{314–342}$ are detectable. Spectrum anisotropy increases in all cases, except for 12-PCSL. Inspection of Fig. 5B reveals much stronger effects of the $E1_{314–342}$ insertion in DLPG bilayers. The perturbation is evident for all the spin labels; particularly, in the case of 12-PCSL there is an appearance of a second, more motionally restricted component, indicating that the peptide penetrates appreciably into the membrane interior.

The outer hyperfine splitting, $2A_{max}$, is a reliable and easy-to-perform estimate of the segmental chain mobility. $2A_{max}$ is defined as separation, expressed in gauss, between the low-field maximum and the high-field-minimum, and tends to increase with increasing the restriction in local chain mobility. Fig. 6 shows that, for the *n*-PCSL spin labels in DLPC and DLPG bilayers, $2A_{max}$ decreases with increasing *n*. Inspection of the figure also shows that, although the characteristic flexibility gradient with chain position of the fluid lipid bilayer membranes is preserved, the presence of bound $E1_{314–342}$ causes an increase which depends on the bilayer charge. Particularly, in DLPC membranes $2A_{max}$ increases to roughly the same extent (~2 G), at all spin-label chain positions except the deeper one. The $2A_{max}$ increase due to peptide is much higher than in DLPG membranes (~6 G, see Fig. 6A), and moreover is of the same extent at all the spin-label positions, included to deeper one. When compared with several different proteins or polypeptides analyzed in a recent publication [52], the increase of $2A_{max}$ due to the penetration of $E1_{314–342}$ in an anionic bilayer was among the higher ever registered, highlighting a strong interaction and a deep penetration of this peptide in the DLPG bilayer structure.

In order to estimate the stoichiometry of the E1–DLPG interaction we determined the increase in outer hyperfine splitting, $2\Delta A_{max}$, of the 5-position spin-labeled lipids in DLPG membranes as a function of peptide concentration (Fig. 6B). A typical saturation trend is registered: the decrease in lipid chain mobility saturates with a value of $2\Delta A_{max} \approx 6$ G at a mole ratio of added E1 to DLPG of approximately 0.08, which corresponds to approximately 12 lipid

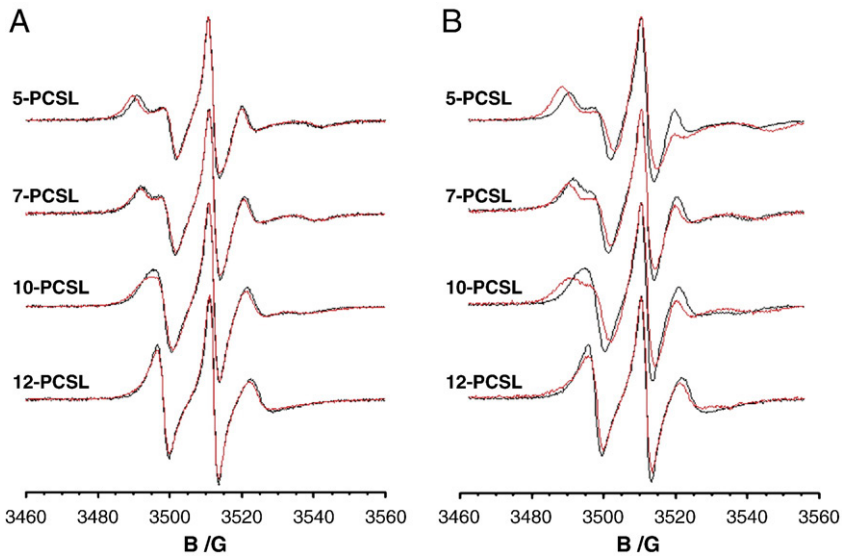

Fig. 5. ESR spectra of *n*-PCSL positional isomers in DLPC (A) and DLPG (B) bilayer membranes, in the presence (red line) and absence (black line) of 1:10 (mol/mol) $E1_{314-342}$.

molecules per peptide. The stoichiometry of the interaction can be estimated alternatively by extrapolation of the increase in $2\Delta A_{max}$, on initial tight binding, to the saturation value of $2\Delta A_{max}$. This gives a value of one E1 molecule bound per 25 lipid molecules. However it should be considered that the latter is likely to be an upper estimate because of a possible nonlinear dependence of $2\Delta A_{max}$ on peptide binding.

4. Discussion

Infection of eukaryotic cells by enveloped viruses requires the fusion of the viral and plasma or endosomal membranes. Highly specific viral envelope glycoproteins catalyze this reaction, thus overcoming its inherent energy barriers. Although the fusion peptide is reported to be the major responsible for the first steps of membrane fusion, other segments of these glycoproteins are indispensable to drive and accomplish the process. Pretransmembrane (PTM) regions, in particular, seem to play an important role as promoters of phospholipid bilayer destabilization, providing a way to lower the energy barrier necessary to fusion [30,33]. The region of the E1 glycoprotein between residues 309 and 340, located in close proximity of the TM domain, is highly conserved in all strains of HCV and is proposed to be involved in membrane destabilization, as well as in pore formation and enlargement, in a manner similar to that of the pretransmembrane and/or loop domains of class I fusion proteins [24].

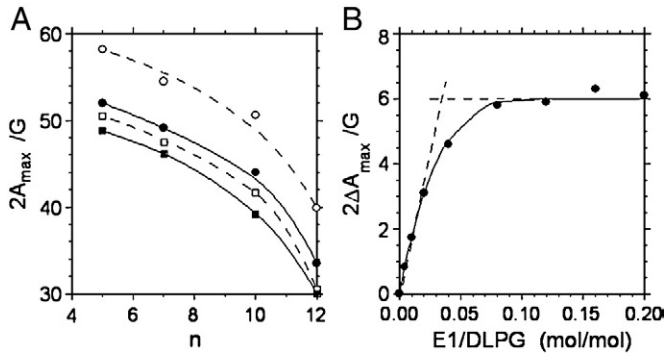

Fig. 6. (A) Dependence on spin-label position, *n*, of the outer hyperfine splitting, $2A_{max}$, of the *n*-PCSL in: DLPC membranes in the absence (■) and presence (□) of 1:10 (mol/mol) $E1_{314-342}$ and DLPG membranes in the absence (●) and presence (○) of 1:10 (mol/mol) E1. (B) Dependence of the increase, $2\Delta A_{max}$, in outer hyperfine splitting of 5-position phospholipid spin labels on the peptide/lipid ratio for $E1_{314-342}$ in DLPG bilayer membranes.

In this paper we have solved for the first time the NMR structure of a peptide corresponding to the 314–342 region of the E1 glycoprotein and, combining several spectroscopic techniques, we have studied his behavior in membrane mimicking media. A preliminary conformational analysis carried out by CD measurements in different experimental conditions suggested that the peptide exhibits a clear propensity to adopt a helical folding in membrane mimicking media with a slight preference to negative charged bilayers.

Tryptophan fluorescence spectra show that the peptide interacts with anionic and zwitterionic phospholipid membranes. In presence of anionic phospholipids the peptide is better incorporated into the membranes whereas in the presence of cholesterol the peptide tends to adsorb on the surface of cholesterol enriched bilayers, independently on their charge.

ESR spectra allowed us a more accurate evaluation of the membrane interaction and insertion of the E1 region selected. The analysis of the ESR data indicates a strong interaction and deep penetration of this peptide in the bilayer structure of the membrane, both in the case of anionic and zwitterionic phospholipid, probably due to the largely apolar character of the peptide structure. Moreover, the interaction with anionic phospholipids is among the strongest ever observed, not only when comparing the data obtained for the same peptide in presence of zwitterionic phospholipids, but also when considering the interactions of several other membrane active proteins and peptides with anionic multilamellar phospholipids [56]. These results indicate that the peptide deeply penetrates the membrane.

According to the CD data, $E1_{314-342}$ peptide in a low polarity environment assumes a partial ordered structure, with a large α-helical character. Among the different experimental conditions explored, we obtained suitable NMR spectra only in the HFIP/H_2O (80/20 v/v), a low polarity mixture that can reproduce an environment close to the inner membrane. It is worth to consider also that this medium represents a good compromise between chemical physical conditions and quality of experimental data, and that was already used to solve the solution structure of other membrane-interacting peptides, including the Amyloid β-peptides A-β-(1–42) and A-β-(25–35) [61,62].

The structure calculated out of the 386 NMR constraints shows two helical stretches encompassing residues 319–323 and 329–338, respectively, interrupted by a break deprived of any canonical

secondary structure. Nevertheless, this region is very well conserved in all the conformers resulting from the structure calculation procedure and is stabilized by a dense network of contacts between the side chains of Trp 326 and Pro 328, and Trp 326 and Ala 331 respectively. It is not new that peptides derived from fusion proteins assume a bended structure in solution, for example, it has been shown that the "fixed angle boomerang structure" of the fusion peptide of influenza hemaglutinin is required to support membrane fusion sufficient to anchor the fusion domain in the proper conformation in the interface of the lipid bilayer [63]. Even more interestingly it was proved that a tryptophan residue is involved in the stabilization of the structure through hydrophobic interactions [64]. Obviously, further experiments will be required to confirm that the bended structure of the E1 peptide is also important for viral entry.

It is also interesting to notice that the second helical stretch (between residues 329 and 338) includes a conserved hydrophobic E1 heptad repeat region (see Table 1) whose mutation is reported [65] to affect dramatically viral entry, while the E1 and E2 heterodimerization is not hampered. More in detail, the mutations V333P L337P completely blocked virus entry while the mutation of the same residues into alanine resulted in a site-specific entry defects. These data, combined with our structure, suggest that the helical conformation is an essential prerequisite for virus entry.

Interaction of domains of the fusion proteins with both the juxtaposed membranes (the viral membrane and that of the target cell) is fundamental for their fusion. Penetration and/or adsorption of peptidic sequences into/onto the lipid bilayer, like those found in the present work, causes a membrane stress, often related to a perturbation in the packing of the lipid molecules [66]. In lack of any datum on the E1 conformational changes and lipid membranes rearrangements during the fusion process, one cannot discriminate which is the membrane the peptide investigated in the present work interact with. Particularly, because of its closeness to the protein TM domain, one cannot exclude that it exerts its main role in the process by interacting with the viral membrane rather then with that of the target cell. Further studies are necessary to clarify this point.

Overall, the structural features and the entrance of the $E1_{314–342}$ peptide in the phospholipids membranes are in agreement with the hypothesis that this region of E1 might play an essential role in membrane fusion, maybe involved in pore formation and enlargement as it has been suggested for class I fusion proteins [25] and consequent viral entry. Furthermore, despite the high variability of HCV envelope protein sequence, this domain of E1 is conserved among the different genotypes, becoming an optimal target for the development of anti-viral molecules.

Acknowledgments

The work was financially supported by European Commission grant LSHB-CT-2007-037435 and by Ministero dell'Istruzione, dell'Università e della Ricerca (FIRB RBNE03B8KK). We thank also the CIMCF (Centro Interdipartimentale di Metodologie Chimico-Fisiche) of the University of Napoli "Federico II for the use of the CD and ESR instruments.

Appendix A. Supplementary data

Supplementary data associated with this article can be found, in the online version, at doi:10.1016/j.bbamem.2009.10.018.

References

[1] W.C. Lemon SM, M.J. Alter, M. Yi, Hepatitis C Virus, in: D.M.K.a.P.M. Howley (Ed.), Fields Virology, Lippincott-Raven, Philadelphia, 2007, pp. 1253–1304.
[2] M.P. Manns, H. Wedemeyer, M. Cornberg, Treating viral hepatitis C: efficacy, side effects, and complications, Gut 55 (2006) 1350–1359.
[3] M.P. Manns, G.R. Foster, J.K. Rockstroh, S. Zeuzem, F. Zoulim, M. Houghton, The way forward in HCV treatment–finding the right path, Nat. Rev. Drug Discov. 6 (2007) 991–1000.
[4] B.D. Lindenbach, H.J. Thiel, C.M. Rice, Flaviviridae: The viruses and their replication, in: D.M.K.a.P.M. Howley (Ed.), Fields Virology, Lippincott-Raven, Philadelphia, 2007, pp. 1101–1152.
[5] J. Dubuisson, Hepatitis C virus proteins, World J. Gastroenterol. 13 (2007) 2406–2415.
[6] V. Lohmann, F. Korner, J. Koch, U. Herian, L. Theilmann, R. Bartenschlager, Replication of subgenomic hepatitis C virus RNAs in a hepatoma cell line, Science 285 (1999) 110–113.
[7] V. Jirasko, R. Montserret, N. Appel, A. Janvier, L. Eustachi, C. Brohm, E. Steinmann, T. Pietschmann, F. Penin, R. Bartenschlager, Structural and Functional Characterization of Nonstructural Protein 2 for Its Role in Hepatitis C Virus Assembly, J. Biol. Chem. 283 (2008) 28546–28562.
[8] E. Steinmann, F. Penin, S. Kallis, A.H. Patel, R. Bartenschlager, T. Pietschmann, Hepatitis C virus p7 protein is crucial for assembly and release of infectious virions, PLoS Pathog. 3 (2007) e103.
[9] B. Bartosch, J. Dubuisson, F.L. Cosset, Infectious hepatitis C virus pseudo-particles containing functional E1-E2 envelope protein complexes, J. Exp. Med. 197 (2003) 633–642.
[10] F. Helle, J. Dubuisson, Hepatitis C virus entry into host cells, Cell. Mol. Life. Sci. 65 (2008) 100–112.
[11] V. Deleersnyder, A. Pillez, C. Wychowski, K. Blight, J. Xu, Y.S. Hahn, C.M. Rice, J. Dubuisson, Formation of native hepatitis C virus glycoprotein complexes, J. Virol. 71 (1997) 697–704.
[12] A. Op De Beeck, L. Cocquerel, J. Dubuisson, Biogenesis of hepatitis C virus envelope glycoproteins, J. Gen. Virol. 82 (2001) 2589–2595.
[13] A. Op De Beeck, C. Voisset, B. Bartosch, Y. Ciczora, L. Cocquerel, Z. Keck, S. Foung, F.L. Cosset, J. Dubuisson, Characterization of functional hepatitis C virus envelope glycoproteins, J. Virol. 78 (2004) 2994–3002.
[14] B. Bartosch, F.L. Cosset, Studying HCV Cell Entry with HCV Pseudoparticles (HCVpp), Methods Mol. Biol. 510 (2009) 279–293.
[15] T. Wakita, T. Pietschmann, T. Kato, T. Date, M. Miyamoto, Z. Zhao, K. Murthy, A. Habermann, H.G. Krausslich, M. Mizokami, R. Bartenschlager, T.J. Liang, Production of infectious hepatitis C virus in tissue culture from a cloned viral genome, Nat. Med. 11 (2005) 791–796.
[16] J. Zhong, P. Gastaminza, G. Cheng, S. Kapadia, T. Kato, D.R. Burton, S.F. Wieland, S.L. Uprichard, T. Wakita, F.V. Chisari, Robust hepatitis C virus infection in vitro, Proc. Natl. Acad. Sci. U. S. A. 102 (2005) 9294–9299.
[17] B.D. Lindenbach, M.J. Evans, A.J. Syder, B. Wolk, T.L. Tellinghuisen, C.C. Liu, T. Maruyama, R.O. Hynes, D.R. Burton, J.A. McKeating, C.M. Rice, Complete replication of hepatitis C virus in cell culture, Science 309 (2005) 623–626.
[18] P. Pileri, Y. Uematsu, S. Campagnoli, G. Galli, F. Falugi, R. Petracca, A.J. Weiner, M. Houghton, D. Rosa, G. Grandi, S. Abrignani, Binding of hepatitis C virus to CD81, Science 282 (1998) 938–941.
[19] M.J. Evans, T. von Hahn, D.M. Tscherne, A.J. Syder, M. Panis, B. Wolk, T. Hatziioannou, J.A. McKeating, P.D. Bieniasz, C.M. Rice, Claudin-1 is a hepatitis C virus co-receptor required for a late step in entry, Nature 446 (2007) 801–805.
[20] B.D. Lindenbach, P. Meuleman, A. Ploss, T. Vanwolleghem, A.J. Syder, J.A. McKeating, R.E. Lanford, S.M. Feinstone, M.E. Major, G. Leroux-Roels, C.M. Rice, Cell culture-grown hepatitis C virus is infectious in vivo and can be recultured in vitro, Proc. Natl. Acad. Sci. U. S. A. 103 (2006) 3805–3809.
[21] K.B. Rothwangl, B. Manicassamy, S.L. Uprichard, L. Rong, Dissecting the role of putative CD81 binding regions of E2 in mediating HCV entry: putative CD81 binding region 1 is not involved in CD81 binding, Virol. J. 5 (2008) 46.
[22] D. Lavillette, B. Bartosch, D. Nourrisson, G. Verney, F.L. Cosset, F. Penin, E.I. Pecheur, Hepatitis C virus glycoproteins mediate low pH-dependent membrane fusion with liposomes, J. Biol. Chem. 281 (2006) 3909–3917.
[23] F. Penin, J. Dubuisson, F.A. Rey, D. Moradpour, J.M. Pawlotsky, Structural biology of hepatitis C virus, Hepatology 39 (2004) 5–19.
[24] A.J. Perez-Berna, A. Bernabeu, M.R. Moreno, J. Guillen, J. Villalain, The pre-transmembrane region of the HCV E1 envelope glycoprotein: interaction with model membranes, Biochim. Biophys. Acta 1778 (2008) 2069–2080.
[25] A.J. Perez-Berna, M.R. Moreno, J. Guillen, A. Bernabeu, J. Villalain, The membrane-active regions of the hepatitis C virus E1 and E2 envelope glycoproteins, Biochemistry 45 (2006) 3755–3768.
[26] D. Lavillette, E.I. Pecheur, P. Donot, J. Fresquet, J. Molle, R. Corbau, M. Dreux, F. Penin, F.L. Cosset, Characterization of fusion determinants points to the involvement of three discrete regions of both E1 and E2 glycoproteins in the membrane fusion process of hepatitis C virus, J. Virol. 81 (2007) 8752–8765.
[27] S.G. Peisajovich, Y. Shai, Viral fusion proteins: multiple regions contribute to membrane fusion, Biochim. Biophys. Acta. 1614 (2003) 122–129.
[28] M. Lorizate, N. Huarte, A. Saez-Cirion, J.L. Nieva, Interfacial pre-transmembrane domains in viral proteins promoting membrane fusion and fission, Biochim. Biophys. Acta. 1778 (2008) 1624–1639.
[29] T. Suarez, W.R. Gallaher, A. Agirre, F.M. Goni, J.L. Nieva, Membrane interface-interacting sequences within the ectodomain of the human immunodeficiency virus type 1 envelope glycoprotein: putative role during viral fusion, J. Virol. 74 (2000) 8038–8047.
[30] A. Saez-Cirion, J.L. Arrondo, M.J. Gomara, M. Lorizate, I. Iloro, G. Melikyan, J.L. Nieva, Structural and functional roles of HIV-1 gp41 pretransmembrane sequence segmentation, Biophys. J. 85 (2003) 3769–3780.
[31] A. Saez-Cirion, M.J. Gomara, A. Agirre, J.L. Nieva, Pre-transmembrane sequence of Ebola glycoprotein. Interfacial hydrophobicity distribution and interaction with membranes, FEBS Lett. 533 (2003) 47–53.

[32] I. Munoz-Barroso, K. Salzwedel, E. Hunter, R. Blumenthal, Role of the membrane-proximal domain in the initial stages of human immunodeficiency virus type 1 envelope glycoprotein-mediated membrane fusion, J. Virol. 73 (1999) 6089–6092.
[33] T. Suarez, S. Nir, F.M. Goni, A. Saez-Cirion, J.L. Nieva, The pre-transmembrane region of the human immunodeficiency virus type-1 glycoprotein: a novel fusogenic sequence, FEBS Lett. 477 (2000) 145–149.
[34] B. Sainz Jr., J.M. Rausch, W.R. Gallaher, R.F. Garry, W.C. Wimley, The aromatic domain of the coronavirus class I viral fusion protein induces membrane permeabilization: putative role during viral entry, Biochemistry 44 (2005) 947–958.
[35] B. Rost, P. Fariselli, R. Casadio, Topology prediction for helical transmembrane proteins at 86% accuracy, Protein Sci. 5 (1996) 1704–1718.
[36] L. Whitmore, B.A. Wallace, Protein secondary structure analyses from circular dichroism spectroscopy: methods and reference databases, Biopolymers 89 (2008) 392–400.
[37] J. Jeener, B.H. Meyer, P. Bachman, R.R. Ernst, Investigation of exchange processes by two-dimensional NMR spectroscopy, J. Chem. Phys. 71 (1979) 4546–4553.
[38] A. Bax, D.G. Davis, Mlev-17-based two-dimensional homonuclear magnetization transfer spectroscopy, J. Magn. Reson. 65 (1985) 355–360.
[39] S. Macura, R.R. Ernst, Elucidation of cross relaxation in liquids by two-dimensional NMR spectroscopy, Mol. Phys. 41 (1980) 95–117.
[40] L. Braunschweiler, R.R. Ernst, Interactions between Charged Polypeptides and Nonionic Surfactants, J. Magn. Reson. 53 (1983) 521–528.
[41] B.A. Johnson, Using NMRView to visualize and analyze the NMR spectra of macromolecules, Methods Mol. Biol. 278 (2004) 313–352.
[42] P. Guntert, C. Mumenthaler, K. Wuthrich, Torsion angle dynamics for NMR structure calculation with the new program DYANA, J. Mol. Biol. 273 (1997) 283–298.
[43] D.A. Pearlman, D.A. Case, J.W. Caldwell, W.S. Ross, T.E. Cheatham III, S. DeBolt, D. Ferguson, G. Seibel, P.A. Kollman, AMBER, a computer program for applying molecular mechanics, normal mode analysis, molecular dynamics and free energy calculations to elucidate the structures and energies of molecules. Comput. Phys. Commun. 91 (1995) 1–41.
[44] K. Schorn, D. Mars, Extracting order parameters from powder EPR lineshapes for spin-labelled lipids in membranes, Spectrochim. Acta A (1997) 2235–2240.
[45] C. Montigny, F. Penin, C. Lethias, P. Falson, Overcoming the toxicity of membrane peptide expression in bacteria by upstream insertion of Asp-Pro sequence, Biochim. Biophys. Acta. 1660 (2004) 53–65.
[46] S.S. Rawat, M. Viard, S.A. Gallo, A. Rein, R. Blumenthal, A. Puri, Modulation of entry of enveloped viruses by cholesterol and sphingolipids (Review), Mol. Membr. Biol. 20 (2003) 243–254.
[47] K. Weise, J. Reed, Fusion peptides and transmembrane domains of fusion proteins are characterized by different but specific structural properties, Chembiochem 9 (2008) 934–943.
[48] B.D. Lindenbach, B.M. Pragai, R. Montserret, R.K. Beran, A.M. Pyle, F. Penin, C.M. Rice, The C terminus of hepatitis C virus NS4A encodes an electrostatic switch that regulates NS5A hyperphosphorylation and viral replication, J. Virol. 81 (2007) 8905–8918.
[49] S. Konev, Fluorescence and Phosphorescence of Proteins and Acids, (1967).
[50] L. Ambrosone, G. D'Errico, R. Ragone, Interaction of tryptophan and N-acetyltryptophanamide with dodecylpentaoxyethyleneglycol ether micelles, Spectrochim. Acta (1997) 1615–1620.
[51] P. Callis, T. Liu, Quantitative prediction of fluorescence quantum yields for tryptophan in proteins, J. Phys. Chem. B (2004) 4248–4259.
[52] S. Galdiero, A. Falanga, M. Vitiello, H. Browne, C. Pedone, M. Galdiero, Fusogenic domains in herpes simplex virus type 1 glycoprotein H, J. Biol. Chem. 280 (2005) 28632–28643.
[53] D.K. Chang, S.F. Cheng, E.A. Kantchev, C.H. Lin, Y.T. Liu, Membrane interaction and structure of the transmembrane domain of influenza hemagglutinin and its fusion peptide complex, BMC Biol. 6 (2008) 2.
[54] F. Stauffer, M.N. Melo, F.A. Carneiro, F.J. Sousa, M.A. Juliano, L. Juliano, R. Mohana-Borges, A.T. Da Poian, M.A. Castanho, Interaction between dengue virus fusion peptide and lipid bilayers depends on peptide clustering, Mol. Membr. Biol. 25 (2008) 128–138.
[55] L.J. Berliner, Spin Labeling:the next millenium, Plenum press, New York, 1998.
[56] G. D'Errico, A.M. D'Ursi, D. Marsh, Interaction of a peptide derived from glycoprotein gp36 of feline immunodeficiency virus and its lipoylated analogue with phospholipid membranes, Biochemistry 47 (2008) 5317–5327.
[57] M. Ramakrishnan, P.H. Jensen, D. Marsh, Alpha-synuclein association with phosphatidylglycerol probed by lipid spin labels, Biochemistry 42 (2003) 12919–12926.
[58] M.J. Swamy, D. Marsh, Spin-label electron paramagnetic resonance studies on the interaction of avidin with dimyristoyl-phosphatidylglycerol membranes, Biochim. Biophys. Acta 1513 (2001) 122–130.
[59] M. Sankaram, D. Marsh, Protein-lipid interactions with peripheral membrane proteins, Elsevier, Amsterdam, 1993.
[60] G. D'Errico, G. Vitiello, O. Ortona, A. Tedeschi, A. Ramunno, A.M. D'Ursi, Interaction between Alzheimer's Abeta(25-35) peptide and phospholipid bilayers: the role of cholesterol, Biochim. Biophys. Acta 1778 (2008) 2710–2716.
[61] O. Crescenzi, S. Tomaselli, R. Guerrini, S. Salvadori, A.M. D'Ursi, P.A. Temussi, D. Picone, Solution structure of the Alzheimer amyloid beta-peptide (1-42) in an apolar microenvironment. Similarity with a virus fusion domain, Eur. J. Biochem. 269 (2002) 5642–5648.
[62] A.M. D'Ursi, M.R. Armenante, R. Guerrini, S. Salvadori, G. Sorrentino, D. Picone, Solution structure of amyloid beta-peptide (25-35) in different media, J. Med. Chem. 47 (2004) 4231–4238.
[63] A.L. Lai, L.K. Tamm, Locking the kink in the influenza hemagglutinin fusion domain structure, J. Biol. Chem. 282 (2007) 23946–23956.
[64] A.L. Lai, H. Park, J.M. White, L.K. Tamm, Fusion peptide of influenza hemagglutinin requires a fixed angle boomerang structure for activity, J. Biol. Chem. 281 (2006) 5760–5770.
[65] H.E. Drummer, I. Boo, P. Poumbourios, Mutagenesis of a conserved fusion peptide-like motif and membrane-proximal heptad-repeat region of hepatitis C virus glycoprotein E1, J. Gen. Virol. 88 (2007) 1144–1148.
[66] L.V. Chernomordik, M.M. Kozlov, Mechanics of membrane fusion, Nat. Struct. Mol. Biol. 15 (2008) 675–683.
[67] G. Merutka, H.J. Dyson, P.E. Wright, 'Random coil' 1H chemical shifts obtained as a function of temperature and trifluoroethanol concentration for the peptide series GGXGG, J. Biomol. NMR 5 (1995) 14–24.